Nonlinear Voltage Control for Three-Phase DC-AC Converters in Hybrid Systems: An Application of the PI-PBC Method

F. M. Serra [1],* , **L. L. Martín Fernández [1]** , **O. D. Montoya [2,3]** , **W. J. Gil-González [3]** and **J. C. Hernández [4]**

[1]   Automatic Control Laboratory (LCA), Facultad de Ingeniería y Ciencias Agropecuarias, Universidad Nacional de San Luis, Villa Mercedes, San Luis 5730, Argentina; lucasfern@unsl.edu.ar

[2]   Facultad de Ingeniería, Universidad Distrital Francisco José de Caldas, Carrera 7 No. 40B-53, Bogotá D.C. 11021, Colombia; o.d.montoyagiraldo@ieee.org

[3]   Laboratorio Inteligente de Energía, Universidad Tecnológica de Bolívar, km 1 vía Turbaco, Cartagena 131001, Colombia; wjgil@utp.edu.co

[4]   Department of Electrical Engineering, University of Jaén, Campus Lagunillas s/n, Edificio A3, 23071 Jaén, Spain; jcasa@ujaen.es

*   Correspondence: fmserra@unsl.edu.ar

Abstract: In this paper, a proportional-integral passivity-based controller (PI-PBC) is proposed to regulate the amplitude and frequency of the three-phase output voltage in a direct-current alternating-current (DC-AC) converter with an LC filter. This converter is used to supply energy to AC loads in hybrid renewable based systems. The proposed strategy uses the well-known proportional-integral (PI) actions and guarantees the stability of the system by means of the Lyapunov theory. The proposed controller continues to maintain the simplicity and robustness of the PI controls using the Hamiltonian representation of the system, thereby ensuring stability and producing improvements in the performance. The performance of the proposed controller was validated based on simulation and experimental results after considering parametric variations and comparing them with classical approaches.

1. Introduction

1.1. General Context

Hybrid Renewable Based Systems (HRS) are promising alternatives for electricity supply in remote areas and are also known as stand-alone microgrid systems [1]. The objective of the stand-alone microgrids is to provide energies based on green technologies to people in remote areas, permitting them to augment their productive capabilities and enhance their quality of life [2]. This is possible to implement, thanks to the advances in renewable energy technologies that have allowed the installation of power generations in remote areas, which in turn benefit and cover non-interconnected areas.

Stand-alone microgrid systems can include different types of energy sources (photovoltaic and wind) [3], storage systems (battery banks and supercapacitors) [4], and loads. These elements can be connected through alternating current (AC) or direct current (DC) grids. In Reference [5], a comprehensive review of AC and DC microgrids was presented. DC grids are preferred because they have a higher power density than AC grids; in addition, they do not require synchronization and

incur only minor losses due to the skin effect [6]. Figure 1 shows a representative scheme for an HRS where the elements are connected through a DC grid.
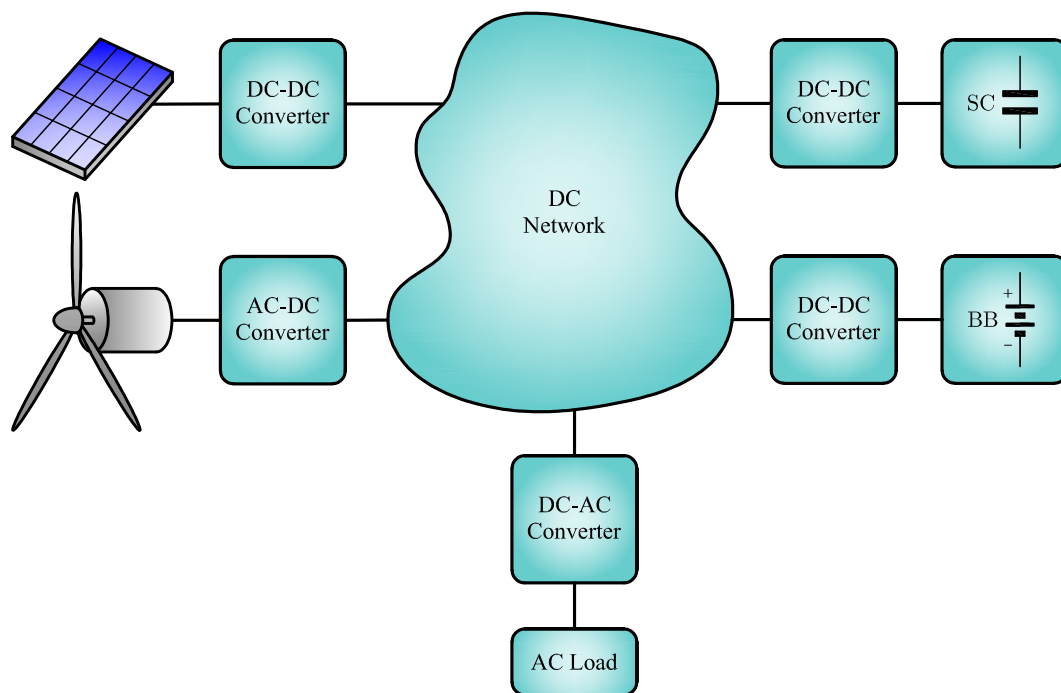
Figure 1. Renewable-based hybrid DC system.

Note that the DC network concept comprehends an extensive range of applications, from high-voltage (examples are given in [7,8]) to low-voltage levels (examples are provided in [9,10]).

In addition, DC networks are especially attractive in control applications since the droop controls of reactive power and frequency disappear in these networks, making it easier for power flow control through lines in high-voltage levels or voltage regulation in low-voltage usages [11]. Another important aspect of the DC network is the possibility of providing service to rural or remote areas with renewable source and energy storage devices, as depicted in Figure 1; this helps improve the living conditions in those areas. In Reference [10], a nonlinear controller for a typical configuration of a rural microgrid was presented and in [12] a comparison between DC and AC microgrids implementations for rural social-economic development was performed.

1.2. Motivation

The interconnection of each part of the system with the DC grid is achieved using power electronics converters, which are responsible for managing the power flow among the sources, storage systems, and loads. In Reference [13,14], examples of the use of the power electronics converters for such interconnections were described. The objective of the power flow control in a hybrid system is to satisfy the energy demand on the loads, maximize the energy extracted from renewable energy sources, and use storage systems efficiently.

The converter is entrusted with controlling the AC voltage applied to the loads, which is usually a DC-AC converter with an LC output filter [15]. This converter can be single-phase or three-phase, depending on the load type. Meanwhile, its control regulates the amplitude and frequency of the output voltage based on a DC voltage applied on the input, which can then be controlled for the remaining HRS [16–18].

The control strategy proposed in this research is motivated by the necessity to have robust and stable control methods for providing sinusoidal voltages in remote areas where conventional power systems are nonexistent [19]. This entails that the opportunity to provide electrical service is by

interfacing renewable energy resources (mainly wind turbines and photovoltaic plants) with power electronic converters that can regulate voltage and frequency by tracking sinusoidal references [20]. The approach that uses sinusoidal references is different from a conventional emulation of synchronous generators via virtual inertia control [21] since it is recommended for weak grids with large frequency variations. In these control schemes, active and reactive power measurements are used to define the frequency and voltage references [20]. Nevertheless, the proposed controller in this paper is focusing on supplying electrical service to linear and non-linear loads directly interfaced with VSCs, which implies that the measures of active and reactive power are not efficient in regulating the output voltage. For this reason, our aim is to have a direct voltage control strategy based on trajectory tracking via passivity-based control approach with experimental validations, allowing supporting three-phase balanced voltages in passive and switched loads.

1.3. Brief State-of-the-Art

In specialized literature, several strategies have been developed for the control of DC-AC converters. Due to their simplicity, the most widely used approaches are based on classic linear controllers, which are proportional-integral (PI) controllers [22]. Even though these strategies are the most used, they cannot guarantee the stability of the system. Additionally, they do not perform well away from the point of operation as in the case of non-linear loads. [16]. Therefore, advanced strategies have been developed to address the poor performance of classic controllers. In Reference [23], a feedback linearization control method was proposed based on a power-balance model between the converter and the load. This method improves the performance of linear and nonlinear loads, but the selection of gains is critical. In Reference [24], a current control algorithm for uninterruptible power supplies based on PID compensator was presented. [25] showed the reduction of voltage distortion caused as a result of slowly varying harmonic currents that use synchronous-frame harmonic regulators.Reference [26] describes an integral resonant controller of the output voltage management arrangement in a three-phase VSI. Reference [27] presented a model predictive control for output voltage regulation of a three-phase inverter with output LC filter feeding linear and nonlinear loads. In addition, authors in [28] use the same control strategy for a single-phase voltage source with linear and nonlinear loads. Despite previous works demonstrating good performance of their objective controls, none of them can guarantee the stability of the system.

On the other hand, the application of passivity-based control (PBC) techniques to power converters has the advantage of providing stable closed-loop controllers with good dynamic behavior. In Reference [16], an interconnection and damping assignment (IDA-PBC) approach was proposed to regulate the output voltage from a DC-AC converter and a comparison was also made with classic controllers. The results of [16] demonstrated the good performance of the proposed controller, even when a nonlinear load was considered. An adaptive robust control method for a DC-AC converter with high dynamic performance under nonlinear and unbalanced loads was also proposed by [29]. In both of these methods, the stability is ensured by the passive properties of the controlled system [30]. The problem with the PBC controllers applied to power converters is that the control laws depend on the system parameters and, so, stable-state errors occur when these parameters vary. The errors caused by variations in the system parameters can be eliminated with different techniques; for e.g., a dynamic extension with an integral action was proposed by [16] but at the expense of increasing the complexity of the system.

PI-PBC controllers have been proposed to combine the advantages (simplicity and robustness) of PI-based designs with the typical stability analysis based on the Lyapunov theorem employed in passive strategies. These controllers have been used in power converters for several applications [31–34].

Authors in [31] have presented the general basis of the PI-PBC theory applied to power electronic converters (switched systems). These authors demonstrate that with PI gains in a Hamiltonian representation of the averaged dynamic of the converter is possible to provide constant direct current–voltage to linear loads. Simulation and experimental results demonstrated that when VSCs

are used in conversion mode (sinusoidal input to DC constant output), the PI-PBC method guarantees asymptotic stability if the load is completely linear (i.e., resistive). Observe that the VSC was operated with sinusoidal voltage imposed on the AC side to generate constant DC voltage. This is a different case, compared to the approach presented in this paper as we work with constant DC voltage provided by a combination of batteries and renewables to support three-phase balanced voltage in linear and nonlinear loads, guaranteeing stability conditions in the sense of Lyapunov. In reference [32], a general design using the PI-PBC method was presented for tracking trajectories in power electronic converters (sinusoidal or constant references) if they are bounded and differentiable (i.e., admissible trajectories). The stability in closed-loop is ensured via Barbalat's lemma. The authors of this paper validate their control design in an interleaved boost and the modular multilevel converter, including simulation and experimental validations. Note that the first converter works with AC input to provide a constant DC output, while the second one generates single-phase voltages in linear loads considering a constant DC input. This implies that the application of the developed PI-PBC method is different from our approach since we work with the isolated network applications to generate three-phase voltage signals in linear and nonlinear loads. The authors in [33] presented a methodology based on dynamic power compensation of active and reactive power in transmission systems considering superconducting coils integrated via a cascade connection between DC-DC chopper converter and the VSC. The control for this system is developed with PI-PBC, guaranteeing stability in closed-loop. The main aim of this paper is to compensate subsynchronous oscillations in power systems when faults occur in the power grid. Note that the proposal of these authors works with the VSC connected to the grid by controlling active and reactive power flow; while in our approach, the power grid is non-existent and the objective is to provide voltage service to isolated loads, i.e., we generate the power system node with constant voltage and frequency via PI-PBC design. In [34], standard passivity-based control design for integrating renewable energy resources in power systems was developed. The main idea of [34] is to provide a stable control design via PBC, which is made via energy functions using a Lagrangian formulation. Additionally, it is assumed that the wind generator would be connected to the power grid. This implies that the electrical network supports the voltage on the AC side of the converter. For this reason, the authors of this study focused on active and reactive power control and not on the three-voltage generation for isolated power applications as the case studied in our contribution.

In Reference [35], a general control design of controllers for single-phase network applications was presented via interconnection and damping assignment PBC and PI-PBC approaches. In this work, the authors considered isolated power grids composed of batteries, wind turbines, photovoltaic plants, and energy storage devices composed of superconducting coils and supercapacitors. The main contribution in [35] was to demonstrate stability in single-phase networks under well-defined load conditions. Even if this research uses isolated systems by applying PI-PBC control, it is different from our contribution since, in our work, the grid has a three-phase structure and the loads are strong, nonlinear loads (switched devices), which were not considered in [35]. Note that in [36] the initial design based on PI-PBC and IDA-PBC was complemented with modifications on the controller structure to integrate renewables in single-phase networks. In addition, the difference with our approach is that the authors do not present any experimental test that validates their simulation analysis.

Authors in Reference [37] presented a general stability analysis for single-phase networks feed-through power electronic converters considering constant power load. This analysis was performed assuming a Hamiltonian representation of the system and the perfect operation of the controllers that manage the power flow between the distributed energy resources and the grid. The authors of this work do not mention how this approach is extensible to AC grids with strong nonlinear loads as the case study in our proposal.

Even if controllers based on PI-PBC have been proposed for controlling power, electronic converters in single-phase and three-phase applications. In this paper, we focus on the problem of the voltage generation in three-phase nonlinear loads located in isolated areas by deriving the

PI-PBC approach from the classical IDA-PBC method [16], which has not been reported in the scientific literature yet. In addition, our work contains multiple simulation scenarios and some experimental validations that validate the proposed approach, demonstrating its easy implementation in real-life operative cases that combine renewables, batteries, power converters, and nonlinear loads.

It is important to mention that it is necessary to employ optimal tuning of the PI gains so that PI controllers (including classical PI and PI-PBC approaches) perform excellently [38]. Active/passive tuning methods have been reported in the scientific literature. In Reference [39], it was presented an interactive tool for adjusting PI controls in first-order systems from a graphical point of view for first-order systems with time delays, numerical results confirm the efficiency of the tool developed in comparison with other literature reports. In Reference [40], an algorithm for the PID controller based on the gain margin and phase margin concept was presented. However, the controller parameters depend on a single parameter, these parameters are subjected to the desired phase margin, and a minimum required gain margin constraint. The main advantage of these tuning an approach with respect to previous works is that it is easy to implement applicable to any linear as well non-linear model structures. Authors of [41] have presented a simple method to design PI controllers in the frequency domain by proposing an optimization model with constraints. This method uses a single tuning parameter, defined as the quotient between the final crossover frequency and the zero of the controller. This adjusting procedure maximizes the controller gain by considering the equality constraint on the phase margin and an inequality restriction in the gain margin. Numerical results confirm the effectiveness of this proposal in comparison with literature reports. Additional methods for tuning PI controllers have been reported in specialized literature, some of them are particle swarm optimization [42], ant-lion optimizer [43], genetic algorithms [44], and so on. The main feature of these metaheuristic optimization methods is that they work with the minimization of integral indices to find the optimal set of control gains by using sequential programming methods [45].

Remark 1. *The selection of control gains is an important task in the design of PI controllers in power converter applications. These methods can be passive or active approaches that work with optimization models or desired performances [46]. Nevertheless, in this research, our focus is on presenting a simple controller based on the properties of the passivity theory combined with classical and well-known PI actions to generate ideal three-phase voltages for non-linear loads in isolated areas. This implies that the focus in the grid performance with load variations and no optimal adjusting of the control gains. In this sense, we employ a basic tuning method based on the root locus design approach [47].*

1.4. Contribution and Scope

In the present study, a PI-PBC controller is proposed for regulating the amplitude and frequency of the output voltage in a three-phase DC-AC converter with an LC filter, providing a well-defined sinusoidal service to linear and nonlinear loads by transforming the DC signal from the transmission/distribution network to local loads [48].

The main contribution of this research in the literature reports about the control of VSCs for feeding isolated three-phase loads can be summarized as follows:

- ✓ A passivity-based control design that is easily implementable with the main advantages of the classical PI controllers that allows tracking a sinusoidal trajectory by transforming this into a regulation problem. The proposed PI-PBC design also allows guaranteeing stability conditions based on the Lyapunov theory by applying the properties of the Hamiltonian energy models.
- ✓ The proposed controller can maintain objective controls, which are to regulate constant voltage amplitude and constant frequency although the test system feeds a non-linear load, demonstrating the generation of a robust three-phase balanced signal. This is achieved by avoiding the use of classical phase-locked loops embedded in virtual synchronous emulations that emulates inertia properties in converters.

✓   The experimental validation in a laboratory prototype with a realistic model of the system include switching effects, losses, and a detailed transistor model to feed passive loads and nonlinear ones.

In addition, the performance of the controller under parametric variation is shown, and a comparison with the classic PI controller demonstrates the superiority of the proposal to mitigate the harmonic content produced by non-linear loads.

Regarding the scope of this research, it is important to mention that in the control design as well as in the simulation, experimental validations will be considered unique voltage source converters that are forced to work as an ideal voltage source to provide sinusoidal voltages to linear and nonlinear loads. For doing so, we consider that the DC side of the converter is fed by a strong DC network (transmission/distribution DC grid) or by a combination of renewable energy resources and batteries [19,28]. In addition, to determine the amount of instantaneous power absorbed by the load (linear and nonlinear), it is considered that there is a current measure at the load side which is important since the amount of current provided by the converter is a linear function of the load consumption. This implies that the existence of this measure is indispensable when no load estimators are implemented, as in the case studied in this research. Note that the implementation of load estimators could be considered for future work since only a few studies have been reported in the scientific literature with experimental validations.

1.5. Organization of the Document

The remainder of this paper is organized as follows. In Section 2, we describe the configuration of the DC-AC converter and its dynamical modeling using a Hamiltonian representation. In Section 3, we explain the proposed control design based on the PI-PBC approach, which guarantees asymptotic stability according to Lyapunov. In Section 4, we demonstrate the numerical performance of the proposed method based on simulations and experimental validations using a laboratory prototype. Finally, the main conclusions derived based on this study are presented in Section 5.

2. System Configuration and Dynamical Model

The DC-AC converter comprises of a three-phase voltage source converter with IGBTs ($S_1, \ldots, S_6$) and an LC output filter. Figure 2 shows the structure of the DC-AC converter considered in this study for supplying an arbitrary load (i.e., linear or nonlinear consumption) [49].
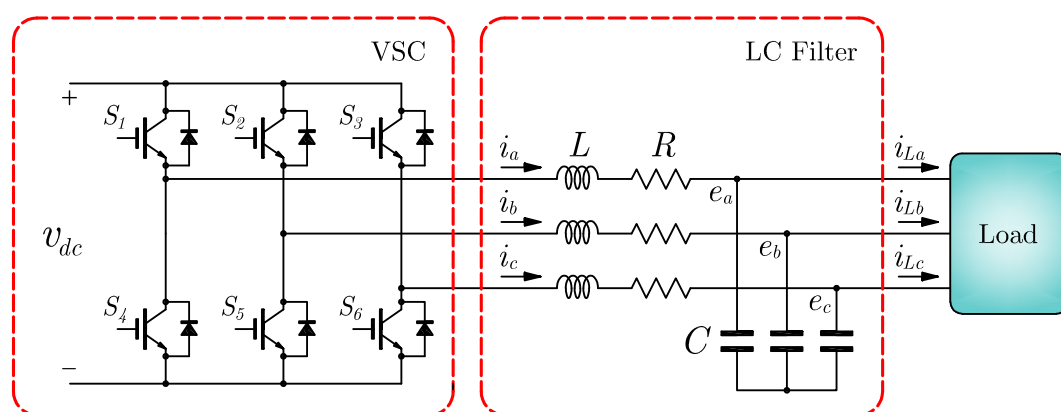

Figure 2. Three-phase DC-AC converter structure.

The DC-link voltage, v_{dc}, is considered to be approximately constant and controlled by other converters involved in the HRS shown in Figure 1, and thus, its dynamics are not considered in our model [16,49].

2.1. Dynamical Model

The DC-AC converter model in dq coordinates is as follows [3],

$$
\begin{aligned}
L\dot{i}_d &= m_d v_{dc} - R i_d - \omega_{dq} L i_q - e_d, & (1) \\
L\dot{i}_q &= m_q v_{dc} - R i_q + \omega_{dq} L i_d - e_q, & (2) \\
C\dot{e}_d &= i_d - \omega_{dq} C e_q - i_{Ld}, & (3) \\
C\dot{e}_q &= i_q + \omega_{dq} C e_d - i_{Lq}, & (4)
\end{aligned}
$$

where ω_{dq} is the angular frequency of the dq reference frame, which is set equal to the desired output-voltage frequency; i_d and i_q represent the currents in the dq frame; e_d and e_q are the output voltages; i_{Ld} and i_{Lq} correspond to the load currents; and m_d and m_q are the inverter modulation indexes. All the variables represented in the dq reference frame are obtained through Park's transformation from the abc variables. The parameters L, C, and R represent the inductance, capacitance of the output filter, and equivalent output resistance, which model the filter inductance losses and converter losses, respectively.

The port-Hamiltonian (pH) model of the system can be written as follows:

$$
\dot{\mathbf{x}} = [\mathbf{J} - \mathbf{R}] \frac{\partial H(\mathbf{x})}{\partial \mathbf{x}} + \mathbf{g}\mathbf{u} + \zeta, \tag{5}
$$

where the state vector is $\mathbf{x}$, $\mathbf{J}$, and $\mathbf{R}$ are the interconnection and damping matrices, respectively, $H(\mathbf{x})$ represents the total energy stored in the system, $\mathbf{g}$ is the input matrix, $\mathbf{u}$ is the control input vector, and ζ represents the external input.

The pH model of the DC-AC converter is represented by Equation (6).

$$
\begin{bmatrix} L\dot{i}_d \\ L\dot{i}_q \\ C\dot{e}_d \\ C\dot{e}_q \end{bmatrix} = \begin{bmatrix} -R & -\omega_{dq}L & -1 & 0 \\ \omega_{dq}L & -R & 0 & -1 \\ 1 & 0 & 0 & -\omega_{dq}C \\ 0 & 1 & \omega_{dq}C & 0 \end{bmatrix} \begin{bmatrix} i_d \\ i_q \\ e_d \\ e_q \end{bmatrix} + \begin{bmatrix} v_{dc} & 0 \\ 0 & v_{dc} \\ 0 & 0 \\ 0 & 0 \end{bmatrix} \begin{bmatrix} m_d \\ m_q \end{bmatrix} + \begin{bmatrix} 0 \\ 0 \\ -i_{Ld} \\ -i_{Lq} \end{bmatrix}. \tag{6}
$$

In this case, the interconnection and damping matrices are defined based on Equation (6) as

$$
\mathbf{J} = \begin{bmatrix} 0 & -\omega_{dq}L & -1 & 0 \\ \omega_{dq}L & 0 & 0 & -1 \\ 1 & 0 & 0 & -\omega_{dq}C \\ 0 & 1 & \omega_{dq}C & 0 \end{bmatrix}, \tag{7}
$$

$$
\mathbf{R} = \begin{bmatrix} R & 0 & 0 & 0 \\ 0 & R & 0 & 0 \\ 0 & 0 & 0 & 0 \\ 0 & 0 & 0 & 0 \end{bmatrix}, \tag{8}
$$

where $\mathbf{J} = -\mathbf{J}^T$ is antisymmetric and $\mathbf{R} = \mathbf{R}^T \geq 0$ is symmetric positive semidefinite.

The total energy stored in the system, $H(\mathbf{x})$, is shown by the sum of the energy stored on the output-filter inductors and capacitors,

$$
H(\mathbf{x}) = \frac{1}{2} \left(L i_d^2 + L i_q^2 + C e_d^2 + C e_q^2 \right). \tag{9}
$$

It should be noted that $H(\mathbf{x})$ is a hyperboloidal function that is convex and positive definite.

3. PI-PBC Approach

This section presents three main aspects of power electronic converters' control using passivity-based control theory. (1) The design of the proposed PI-PBC approach by transforming the trajectory tracking problem into a regulation problem using the incremental representation. (2) The control objective of the problem, i.e., the definition of the desired sinusoidal trajectory. (3) The stability analysis of the proposed control scheme via Lyapunov's stability theorem for autonomous dynamical systems. In the next subsections, each of these aspects will be discussed.

3.1. Control Design

The proposed PI-PBC approach depends on the existence of an admissible trajectory, defined as [34],

$$\mathbf{x}^* = \begin{bmatrix} Li_d^* & Li_q^* & Ce_d^* & Ce_q^* \end{bmatrix}^T, \tag{10}$$

such that the dynamical system in Equation (6) is continuous, differentiable, and bounded, which implies that

$$\dot{\mathbf{x}}^* = [\mathbf{J} - \mathbf{R}] \frac{\partial H(\mathbf{x}^*)}{\partial \mathbf{x}^*} + \mathbf{g}\mathbf{u}^* + \zeta, \tag{11}$$

with some $\mathbf{u}^*$ bounded.

If we define $\tilde{\mathbf{x}} = \mathbf{x} - \mathbf{x}^*$ and $\tilde{\mathbf{u}} = \mathbf{u} - \mathbf{u}^*$, the system in Equation (5) can be written as follows:

$$\dot{\tilde{\mathbf{x}}} + \dot{\mathbf{x}}^* = [\mathbf{J} - \mathbf{R}] \frac{\partial H(\tilde{\mathbf{x}} + \mathbf{x}^*)}{\partial(\tilde{\mathbf{x}} + \mathbf{x}^*)} + \mathbf{g}(\tilde{\mathbf{u}} + \mathbf{u}^*) + \zeta. \tag{12}$$

The energy function of the system given by Equation (9) can be represented as:

$$H(\mathbf{x}) = H(\tilde{\mathbf{x}} + \mathbf{x}^*) = \frac{1}{2}\mathbf{x}^T\mathbf{P}^{-1}\mathbf{x} = \frac{1}{2}(\tilde{\mathbf{x}} + \mathbf{x}^*)^T\mathbf{P}^{-1}(\tilde{\mathbf{x}} + \mathbf{x}^*), \tag{13}$$

and the gradient of this function is,

$$\frac{\partial H(\mathbf{x})}{\partial \mathbf{x}} = \mathbf{P}^{-1}\mathbf{x}, \tag{14}$$

then,

$$\begin{aligned}\frac{\partial H(\tilde{\mathbf{x}} + \mathbf{x}^*)}{\partial(\tilde{\mathbf{x}} + \mathbf{x}^*)} &= \mathbf{P}^{-1}(\tilde{\mathbf{x}} + \mathbf{x}^*) = \mathbf{P}^{-1}\tilde{\mathbf{x}} + \mathbf{P}^{-1}\mathbf{x}^* \\ &= \frac{\partial H(\tilde{\mathbf{x}})}{\partial\tilde{\mathbf{x}}} + \frac{\partial H(\mathbf{x}^*)}{\partial\mathbf{x}^*}.\end{aligned} \tag{15}$$

Using Equation (15), the system defined by Equation (12) can be written as follows:

$$\dot{\tilde{\mathbf{x}}} + \dot{\mathbf{x}}^* = [\mathbf{J} - \mathbf{R}] \frac{\partial H(\tilde{\mathbf{x}})}{\partial\tilde{\mathbf{x}}} + [\mathbf{J} - \mathbf{R}] \frac{\partial H(\mathbf{x}^*)}{\partial\mathbf{x}^*} + \mathbf{g}\tilde{\mathbf{u}} + \mathbf{g}\mathbf{u}^* + \zeta, \tag{16}$$

Thus, the following error dynamics are reached.

$$\dot{\tilde{\mathbf{x}}} = [\mathbf{J} - \mathbf{R}] \frac{\partial H(\tilde{\mathbf{x}})}{\partial\tilde{\mathbf{x}}} + \mathbf{g}\tilde{\mathbf{u}}. \tag{17}$$

In addition, the output of the system can be calculated as follows:

$$\tilde{\mathbf{y}} = \mathbf{g}^T \frac{\partial H(\tilde{\mathbf{x}})}{\partial(\tilde{\mathbf{x}})}. \tag{18}$$

The system in Equation (17) is passive if $\dot{H}(\tilde{\mathbf{x}}) \leq \tilde{\mathbf{y}}^T \tilde{\mathbf{u}}$ [33,34]. Therefore, to obtain a closed-loop dynamic based on Lyapunov theory, the energy function is shown as:

$$H(\tilde{\mathbf{x}}) = \frac{1}{2}\tilde{\mathbf{x}}^T \mathbf{P}^{-1}\mathbf{x}, \tag{19}$$

where $H(0) = 0$ and $H(\tilde{\mathbf{x}}) > 0$, $\forall \tilde{\mathbf{x}} \neq 0$, which satisfy the first and second conditions of the Lyapunov theorem. The time derivative of the proposed energy function is

$$\begin{aligned}
\dot{H}(\tilde{\mathbf{x}}) &= \tilde{\mathbf{x}}^T \mathbf{P}^{-1}\dot{\tilde{\mathbf{x}}} = -\tilde{\mathbf{x}}^T \mathbf{P}^{-1}\mathbf{R}\mathbf{P}^{-1}\tilde{\mathbf{x}} + \tilde{\mathbf{x}}^T \mathbf{P}^{-1}\mathbf{g}\tilde{\mathbf{u}}, \\
&= -\tilde{\mathbf{x}}^T \mathbf{P}^{-1}\mathbf{R}\mathbf{P}^{-1}\tilde{\mathbf{x}} + \tilde{\mathbf{y}}^T \tilde{\mathbf{u}} \leq \tilde{\mathbf{y}}^T \tilde{\mathbf{u}},
\end{aligned} \tag{20}$$

which proves that the dynamics of the error are also passive.

The proposed controller can be written as follows:

$$\begin{aligned}
\dot{\mathbf{z}} &= -\tilde{\mathbf{y}}, \tag{21} \\
\tilde{\mathbf{u}} &= -K_P\tilde{\mathbf{y}} + K_I\mathbf{z}, \tag{22}
\end{aligned}$$

and it has a PI structure, where K_P and K_I are the proportional and integral gain matrices, respectively, which are diagonal and positive definite, and $\tilde{\mathbf{y}}$ is

$$\tilde{\mathbf{y}} = \mathbf{g}^T \frac{\partial H(\tilde{\mathbf{x}})}{\partial \tilde{\mathbf{x}}} = \begin{bmatrix} v_{dc}\left(i_d - i_d^*\right) \\ v_{dc}\left(i_q - i_q^*\right) \end{bmatrix}. \tag{23}$$

Note that $\mathbf{z}$ represents a set of auxiliary variables that allow the passive output feedback and the inclusion of an integral action to minimize steady-state errors on the control objective. For more details of the PI-PBC approach for non-affine dynamic systems, refer to [32].

Using Equation (11), the references of the dq axis currents and the modulation index can be obtained as follows:

$$\begin{aligned}
i_d^* &= \omega_{dq}Ce_q^* + i_{Ld}, \tag{24} \\
i_q^* &= -\omega_{dq}Ce_d^* + i_{Lq}, \tag{25} \\
m_d^* &= \frac{1}{v_{dc}}\left(L\dot{i}_d^* + Ri_d^* + \omega_{dq}Li_q^* + e_d^*\right), \tag{26} \\
m_q^* &= \frac{1}{v_{dc}}\left(L\dot{i}_q^* + Ri_q^* - \omega_{dq}Li_d^* + e_q^*\right), \tag{27}
\end{aligned}$$

where we have considered that $\dot{e}_d^* = \dot{e}_q^* = 0$ because e_d^* and e_q^* are constant values in the Park's reference frame.

Figure 3 shows the proposed control scheme. It can be observed that the modulation indexes are obtained using Equations (22) and (23) with Equation (27), and the references e_d^*, e_q^*, and ω_{dq} are selected by the users. The angle θ_{dq} used in the Park's transformations is obtained from $\frac{d\omega_{dq}}{dt}$.
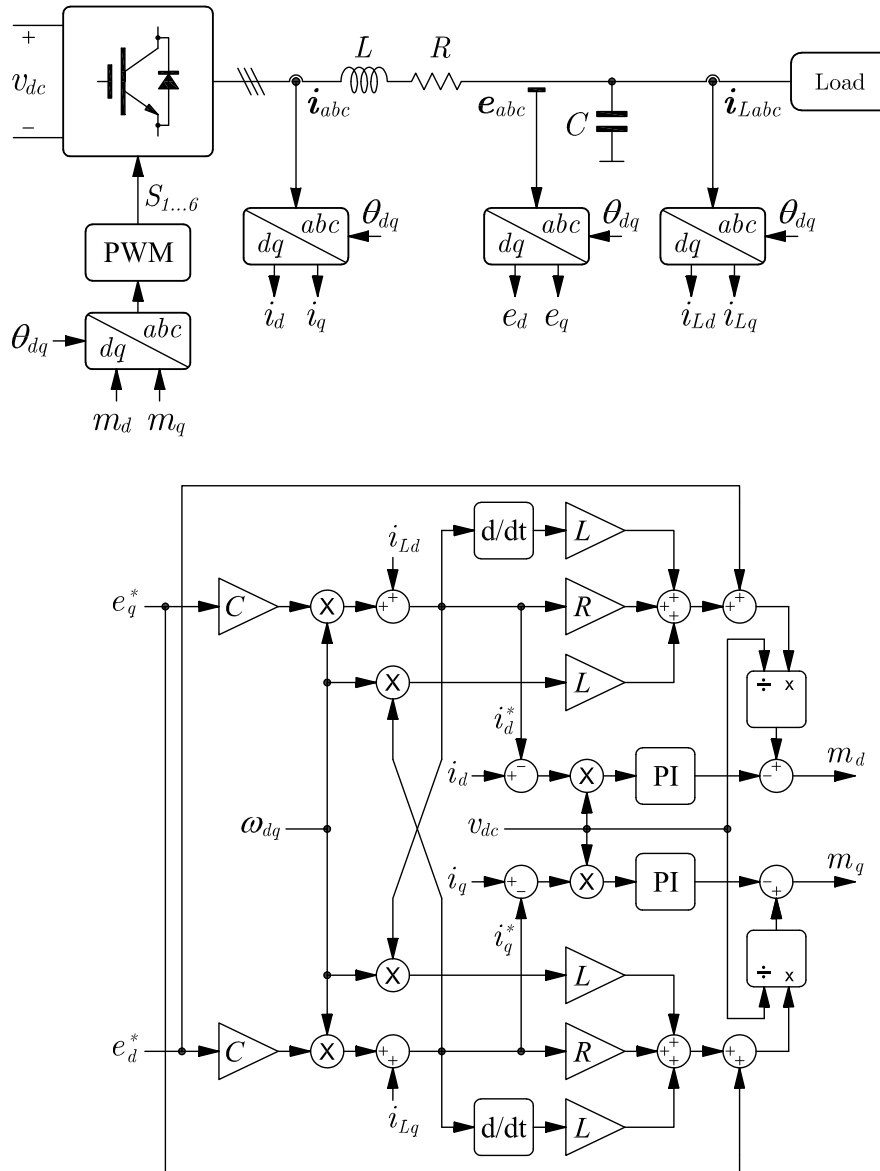
Figure 3. Block diagram of the proposed controller.

3.2. Control Objective

The main idea behind implementing VSCs for the integration of non-linear loads in the AC side using the energy provided by the DC network (see Figure 1) is to generate a three-phase sinusoidal signal with constant amplitude and frequency [19]. This implies that the references for the voltage signals in the capacitors in parallel to the load can be defined as follows:

$$
\begin{aligned}
e_a^*(t) &= \sqrt{2}E_{rms}\sin(\omega t), \\
e_b^*(t) &= \sqrt{2}E_{rms}\sin(\omega t - 2\frac{\pi}{3}), \\
e_c^*(t) &= \sqrt{2}E_{rms}\sin(\omega t + 2\frac{\pi}{3}),
\end{aligned}
\tag{28}
$$

where E_{rms} is the desired voltage magnitude and ω represents the angular frequency, i.e., for this study $\omega = 2\pi f$, with $f = 50$ Hz.

From the desired three-phase voltage reference defined in Equation (28), we can observe that the electrical frequency is considered as an input for the Park's transformation (see Figure 3). This implies

that if the controller makes its task, the voltage outputs in the load will be sinusoidal waves regardless of the load variations (linear or non-linear behavior) [50].

Note that if we send a constant frequency as input to the Parks' transformation, then the sinusoidal references in Equation (28) become constant values in the *dq* reference frame, i.e.,

$$
\begin{aligned}
e_d^*(t) &= E_{rms}, \\
e_q^*(t) &= e_0^*(t) = 0,
\end{aligned}
\tag{29}
$$

which implies that if the controller reaches these values in the *dq* reference frame, then the voltage output will be perfectly sinusoidal in the *abc* reference frame sinusoidal [19].

Remark 2. *Note that the voltage and frequency and regulation reported in this paper allows supporting a three-phase sinusoidal signal in load coupling based on the properties of the controller for following constant references in the dq frame [19]. This is different from classical approaches that regulate voltage and frequency by measuring active and reactive power by emulating synchronous machines using the virtual inertia concept [20,21].*

3.3. Stability Analysis

The stability analysis in modern control applications is an important aspect and should be demonstrated to show that they are suitable for implementation without fails [8,51]; one of the main attractive characteristics of the PBC design is that in a large class of linear and nonlinear system, stability can be guaranteed using Hamiltonian or Lagrangian representations [14,32]. Here, we present basic proof for analyzing the proposed PI-PBC approach, since it was extensively studied in [32,35].

We will enunciate the necessary conditions for guaranteeing stability of a nonlinear autonomous dynamical $\dot{x} = f(x, u)$ system in the sense of Lyapunov around the equilibrium point $x = x^\star$ as follows [52]:

✓　If there is a Lyapunov candidate function $V(x)$ that is positive definite for all $x \neq x^\star$, and zero only for $x = x^\star$, i.e., $V(x) > 0$, $x \neq x^\star$ & $V(x) = 0$, $x = x^\star$,

✓　and the derivative of the Lyapunov function with respect to the time ($\dot{V}(x)$) is negative semidefinite, i.e., ($\dot{V}(x)) \leq 0$, $\forall x \neq x^\star$, & ($\dot{V}(x^\star)) = 0$.

Note that to prove these two necessary conditions for the proposed closed-loop dynamical system with state variables $\tilde{x}$ and z, we employed a quadratic function as recommended in [32] which fulfills the positive definiteness in all the solution space which is zero only in the equilibrium point, as follows:

$$
V(\tilde{\mathbf{x}}, \mathbf{z}) = H(\tilde{\mathbf{x}}) + \frac{1}{2} \mathbf{z}^T K_I \mathbf{z},
\tag{30}
$$

where $H(\tilde{\mathbf{x}})$ is the desired Hamiltonian function. Note that the second term is a quadratic expression as function of the integral variables that deal with these new stable variables introduced by the PI-PBC method [33].

Now, if we take the time derivative of the candidate Lyapunov function in Equation (30), then the following result is yielded:

$$
\dot{V}(\tilde{\mathbf{x}}, \mathbf{z}) = \dot{H}(\tilde{\mathbf{x}}) + \mathbf{z}^T K_I \dot{\mathbf{z}}
\tag{31}
$$

where, if it substitutes the expression in Equation (20) by considering the PI-PBC design in Equation (22), then, the following result is reached:

$$
\begin{aligned}
\dot{V}(\tilde{\mathbf{x}}, \mathbf{z}) &= -\tilde{\mathbf{x}}^T \mathbf{P}^{-1} \mathbf{R} \mathbf{P}^{-1} \tilde{\mathbf{x}} + \tilde{\mathbf{x}}^T \mathbf{P}^{-1} \mathbf{g} \tilde{\mathbf{u}} + \mathbf{z}^T K_I (-\tilde{\mathbf{y}}) \\
&\leq -\tilde{\mathbf{y}}^T K_P \tilde{\mathbf{y}} \leq 0,
\end{aligned}
\tag{32}
$$

which clearly fulfills the second condition of the Lyapunov's theorem [34].

Remark 3. *As the derivative of the Lyapunov function with respect to time does not directly contain the state variables of interest, i.e., $\tilde{x}$ and z, based on the Lyapunov's stability theorem, we can affirm that the dynamical system $\dot{\tilde{x}}$ (see Equation (17)) is stable in a closed-ball that contain the equilibrium point $x = \tilde{x}$, as demonstrated in [35].*

Regarding the range of application of the aforementioned stability analysis of the real systems and its relation to the parameters of the system, it is important to highlight the following facts:

- The PI-PBC design can guarantee stability independently of the value of the parameters of the filter LC since its demonstration is based on the positive definiteness of the matrix **P** in Equation (14) [13]. This matrix is constant and contains at its diagonal the parameters of the filter, which of course are positive in real physical systems. This implies that if there exists variations between the parameters assigned to the controller and the real parameters, it will not compromise the stability of the system in closed-loop [32].
- The control gains assigned to the PI-PBC controller plays an important role in the stability analysis [33]; nevertheless, these need to fulfill an important condition related to the positiveness of their values. Since these are design parameters, we can ensure that they will be positive and the system will remain stable during the closed-loop operation.
- Some unmodeled dynamics such as parasitic resistances in the capacitors connected in parallel to the load or power losses in the converter will help the stable behavior of the system since these parameters introduce additional dampings in the dynamical response of the physical system that we no longer observe in the simulation environment [53].

4. Results

The proposed PI-PBC controller was validated based on simulations and experimental results. The parameters used in the system in both the simulations and experimental tests are listed in Table 1.

Table 1. System parameters.

| Parameter	Value	Unit	Parameter	Value	Unit
Inductance (L)	1.25	mH	Switching frequency (f_s)	20	kHz
Resistance (R)	0.2	Ω	Output frequency (f)	50	Hz
Capacitance (C)	45	μF	DC-link voltage (v_{dc})	311	V
Internal IGBT resistance (R_{on})	10	mΩ	DC-link capacitance (C_{dc})	5400	μF

4.1. Simulation Results

The simulation results were obtained using a realistic model of the system, including the switching effects, losses, and a detailed transistor model. The simulations were implemented using the SimPowerSystem in MATLAB.

To validate the performance of the proposed controller, a test was performed by changing the load (linear and nonlinear). Figure 4a shows the *dq* axis output voltage and its reference, and Figure 4b shows the output voltage and inductor current for phase *a*. Initially, the system operated with a resistive load of 10 Ω, and the reference of the output voltage was $e_d^* = 100$ V and $e_q^* = 0$ V. When the load was changed from 10 Ω to 5 Ω (at 0.1 s), the *d*-axis voltage exhibited a transient variation; this also occurred for the voltage on the *q*-axis, but within a short time (approximately one cycle of the voltage), the controller was able to regulate the amplitude and frequency of the output voltage in the expected time and with the desired dynamic behavior. At 0.2 s, the nonlinear load was connected to the system. Again, the controller regulated the *dq* axis output voltages in an acceptable time and with suitable behavior. In addition, as shown in Figure 4b, the waveform of the voltage was sinusoidal (free of significant harmonics) even under a nonlinear load.
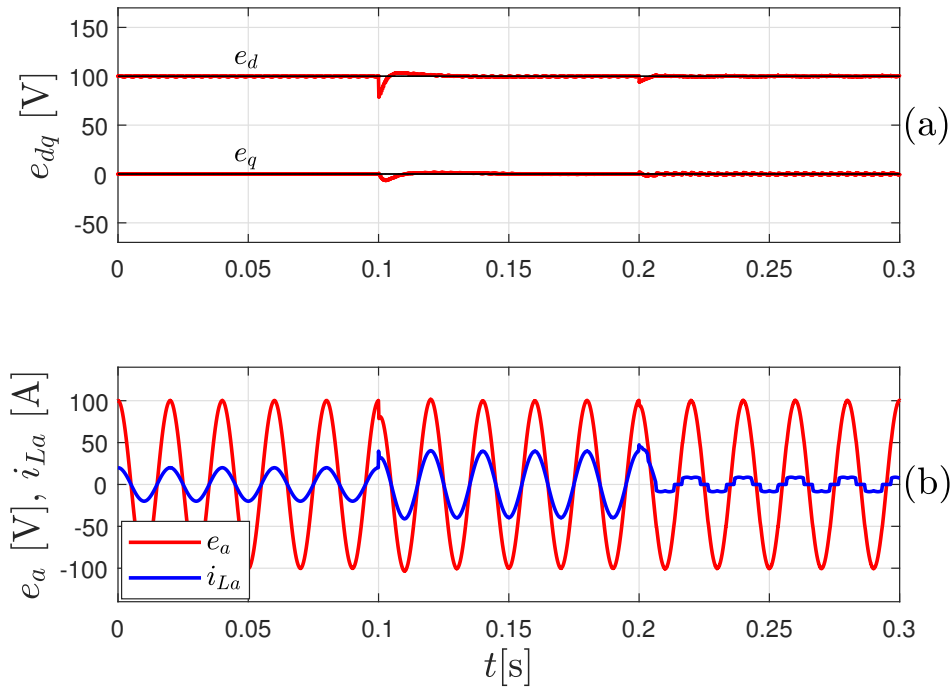
Figure 4. Voltage behavior in the Park's reference frame, and voltage and load current per-phase. (**a**) e_{dq} profile. (**b**) Voltage and load current in phase a.

Figure 5a shows the three-phase output voltage and Figure 5b depicts the currents in the filter inductors. The amplitude of the three-phase output voltage was regulated in advance of the load changes as expected.
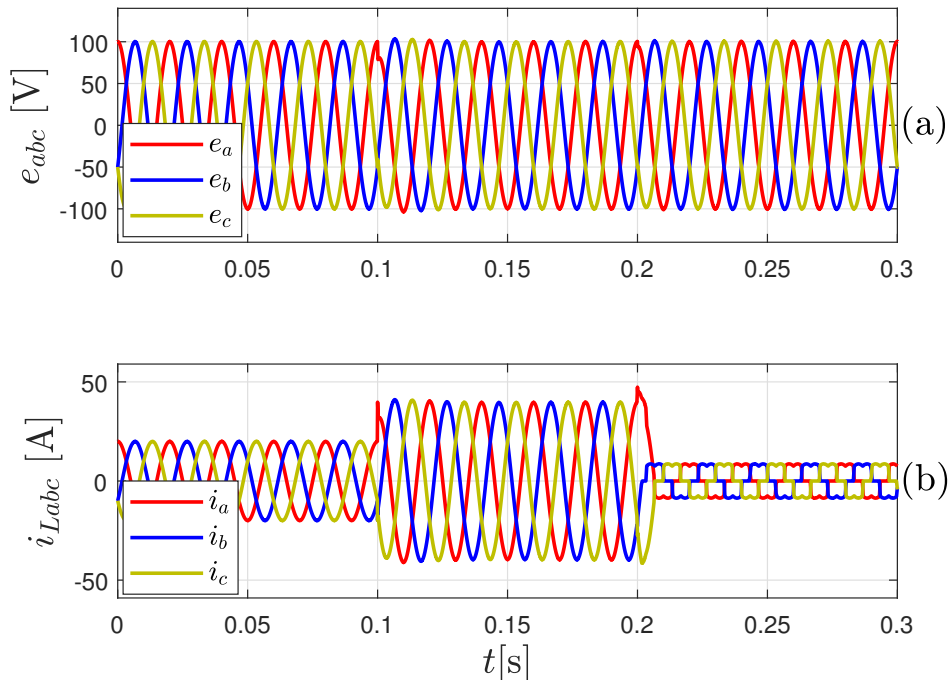
Figure 5. Dynamical performance of the voltage and currents at the point of load connection. (**a**) Three-phase voltage profile. (**b**) Current profile for linear and nonlinear consumption.

With the objective to show the performance of the proposed controller in the presence of parametric variations, a test with varying inductance and resistance values of the LC filter was performed. Figure 6 shows the d-axis output voltage for the same test of Figure 4 when the value of the

inductance and resistance of the filter are different and the same are then considered in the controller. The parameter variation consists of a change of 50% in the inductance and resistance of the filter. It can be observed that the *d*-axis voltage exhibited transient differences between the situations with and without parameter variation, while in regimen, the voltage is regulated in the reference value as the integral action of the PI eliminates possible steady-state errors (see [54]).
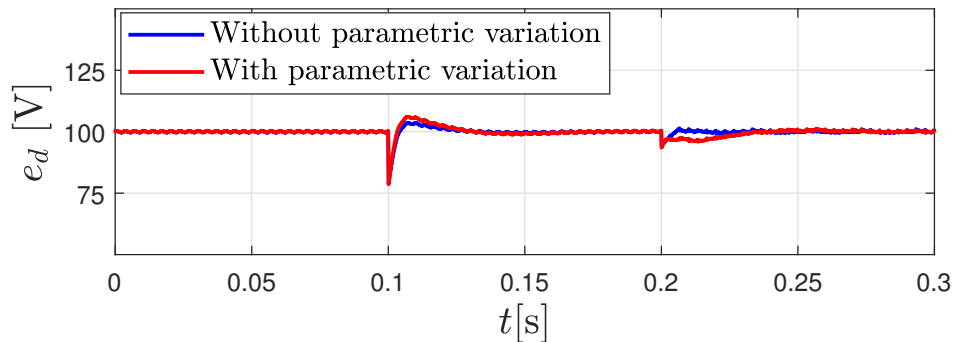

Figure 6. Behavior of *d*-axis voltage for parametric variation.

For comparison purposes with classic approaches (PI controllers), Figure 7 shows the output voltage behavior in *dq*-coordinates for the same test of Figure 4, when a PI controller (in blue) and the proposed PI-PBC controller (in red) are working. It can be observed that the classic PI controller performs similar to PI-PBC when a linear load is considered, but when a non-linear load is connected, the system with the PI controller presents high harmonic content, and therefore the performance is reduced. This test shows the superiority of the proposed strategy to mitigate the harmonics due to non-linear loads.
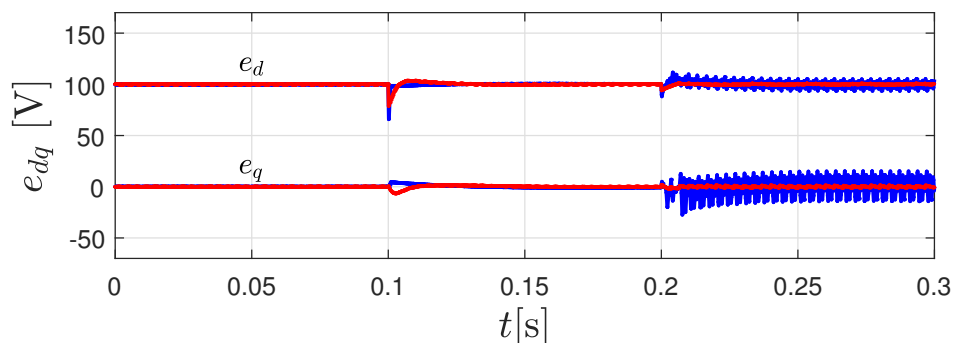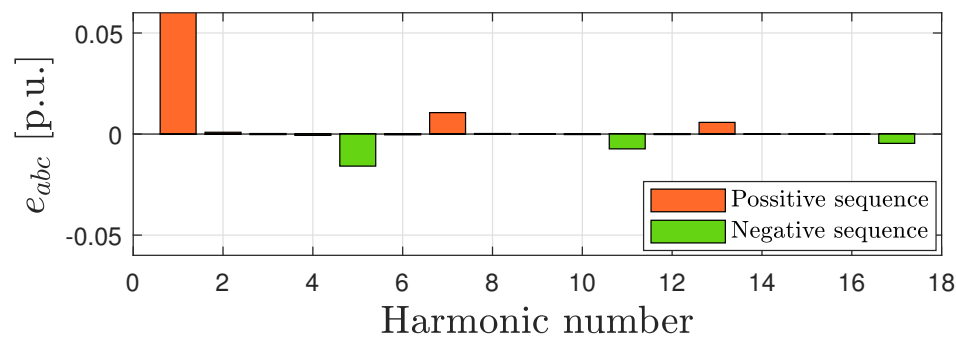

Figure 7. Voltage behavior in the Park's reference frame, comparison between the proposed controller (in red) and the classic PI approach (in blue).

With the aim to demonstrate the performance of the proposed controller under highly demanding conditions, Figure 8 presents a test with a change of the amplitude reference of the output voltage and a change in load when the converter supplies the nonlinear load, as considered in Figure 4. In Figure 8a, the dq axis output voltage and its reference is illustrated and in Figure 8b, the output voltage and inductor current for phase *a* is shown. It can be seen that the proposed PI-PBC controller (in red) regulates the amplitude of the output voltage in the presence of changes of the amplitude reference (0.1 s) and load changes (0.2 s) even when the power of the nonlinear load is increased. Furthermore, in this test, a comparison between the proposed controller (in red) and the classic PI (in yellow) approach was performed. The performance of the classic PI presents high harmonic content as the value of the power of the nonlinear charge increases while the oscillations presented by the PI-PBC are small. It should be noted that the elimination of these oscillations can be accomplished using a multiple reference controller but it will increase the complexity of the control algorithm [24].
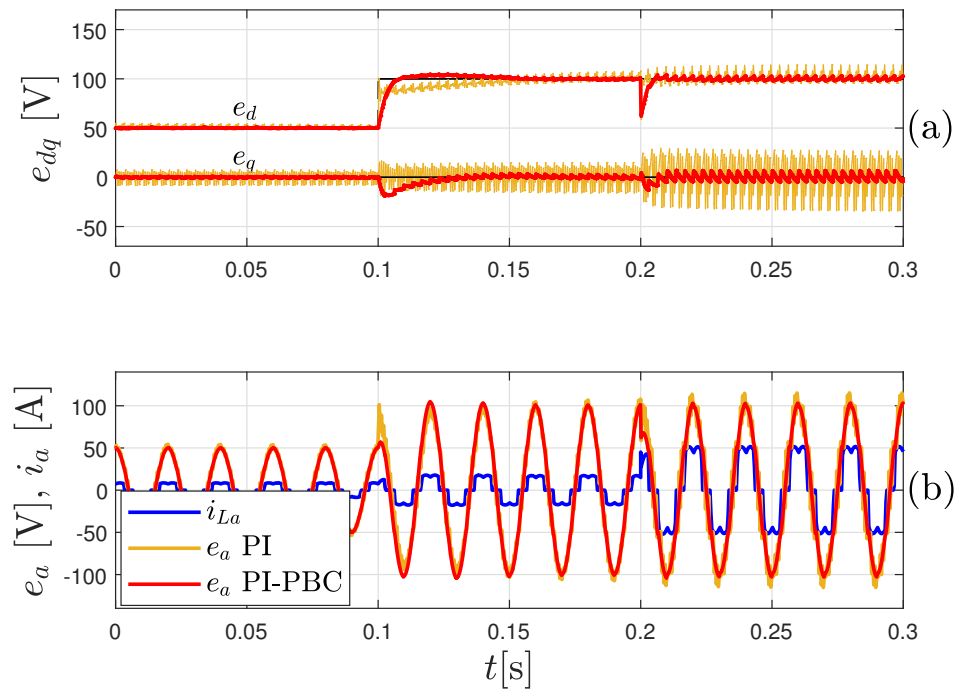
Figure 8. Test system behavior under very demanding conditions for the proposed controller (in red) and the classic PI approach (in yellow). (**a**) Voltage behavior in the Park's reference frame. (**b**) Phase *a* voltage profile.

Figure 9 depicts the harmonic spectrum of the output voltage using the proposed PI-PBC controller. It can be seen that the amplitude of individual harmonics remains below the required limits by the standards and the total harmonic distortion (THD) is 2.17%. This value is lower than the values established by IEC 62040-3 (less than 8%) [16]. Figure 10 shows the harmonic spectrum of the output voltage for the classic PI controller, the THD is 7.37%, which is very close to the allowed limits. The harmonic spectra were obtained for the system feeding the nonlinear load corresponding to Figure 8 between 0.2 s to 0.3 s.

Figure 9. Voltage harmonic spectrums of proportional-integral passivity-based controller (PI-PBC).
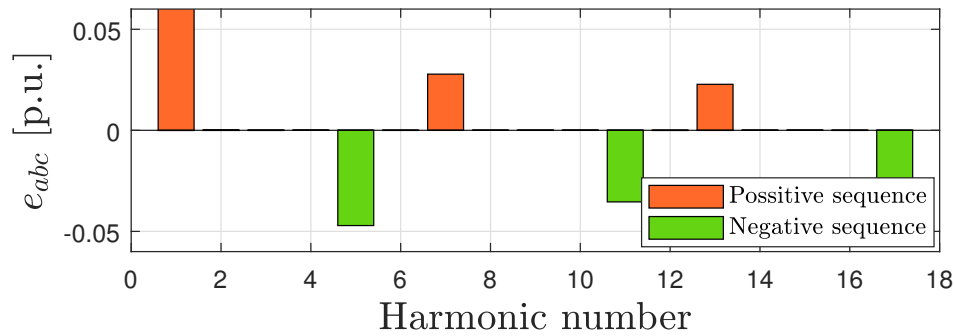
Figure 10. Voltage harmonic spectrums of Classical PI controller.

Finally, Figure 11 shows a test for an unbalanced load. It can be seen that the three-phase voltage is maintained with constant amplitude and frequency, and without significative harmonics when considering these types of loads.
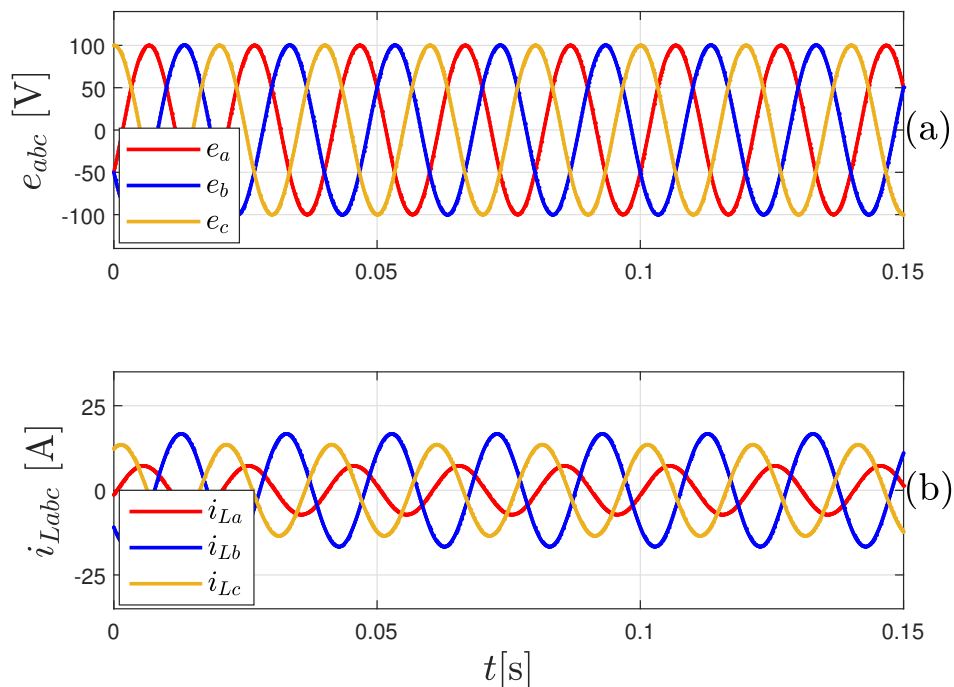

Figure 11. Test system behavior under very demanding conditions for the proposed controller (in red) and the classic PI approach (in yellow). (**a**) Voltage behavior in the Park's reference frame. (**b**) Phase *a* voltage profile.

4.2. Experimental Results

The experimental results were obtained using a laboratory prototype with the same parameters employed in the simulation tests (see Table 1). The DC-AC converter was constructed using an IGBT module (SEMiX101GD12E4s), and the controller was implemented in a TMS320F28335 floating-point DSP (Texas Instruments).

Figure 12 shows the three-phase voltage generated by the system under a resistive load change (50 Ω to 25 Ω). The controller regulated the amplitude and frequency of the output voltage, and the time response required for the load change was approximately one cycle, thereby agreeing with the previously described simulation results, and this time is acceptable in practical applications as well.
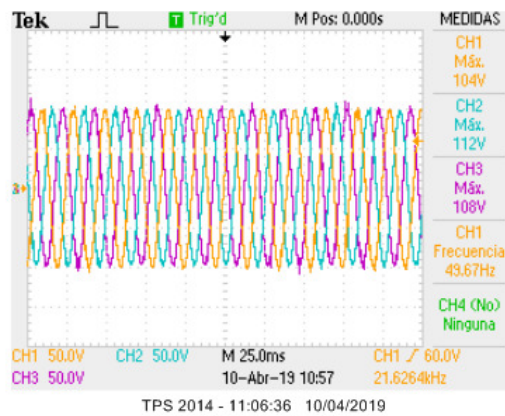
Figure 12. Experimental results: three-phase generated voltage for a resistive load change.

The output voltage and inductor current for phase *a* are shown in Figure 13 for the resistive load change and in Figure 14 for a nonlinear load. The results show that dynamic behavior was acceptable in both cases. In addition, when a nonlinear load was considered (Figure 14), the controller generated an output voltage that was free of significant harmonics. The voltage total harmonic distortion is 3.6%. This value is lower than the values established by IEC 62040-3 (less than 8%) [16].
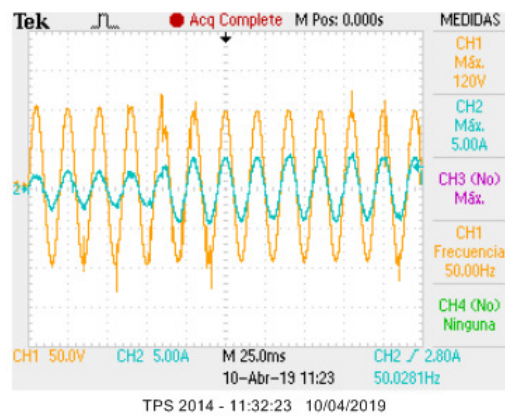

Figure 13. Experimental results: output voltage and inductor current for phase *a* with a resistive load change.
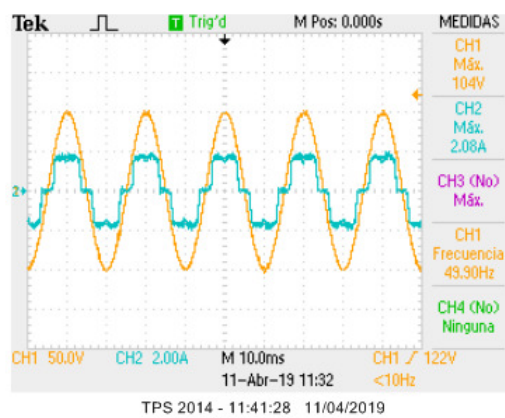

Figure 14. Experimental results: output voltage and inductor current for phase *a* under a nonlinear load.

5. Conclusions

In this article, we present a PI-PBC controller to regulate the amplitude and frequency of a three-phase output voltage in a DC-AC converter with an LC filter. Simulations and experimental results show that the proposed controller allowed regulating the amplitude and frequency of the output voltage of the converter under both linear and nonlinear load changes. Additionally, the PI-PBC allowed generating well-defined sinusoidal signals to linear and nonlinear loads. The results of the performance analysis showed that the proposed design combines the simplicity and robustness of PI-based controllers with the stability and performance characteristics of PBC as a powerful tool for the design of power converter controllers used in hybrid power systems.

Derived from this research, some future recommendations have been made as follows: (1) to develop a direct power control approach to operate DC-AC converters in constant power load applications; (2) to combine the advantages of the passivity-based control designs with virtual inertia emulators to develop robust controllers for weak three-phase distribution networks with unbalanced and nonlinear loads; and (3) to employ advanced methodologies for optimal adjustment of PI control gains using active and passive strategies in order to improve the dynamical performance of the proposed PI-PBC method in applications with large variations in the load terminals.

Abbreviations

The following abbreviations and nomenclature are used in this manuscript:

Acronyms	
AC	Alternating current
BB	Battery
IDA-PBC	Interconnection and damping assignment passivity-based controller
pH	port-Hamiltonian
PI-PBC	Proportional-integral passivity-based controller
DC	Direct current
SC	Supercapacitor
RHS	Renewable-based hybrid systems
Subscripts and superscripts	
$*$	Admissible trajectory
dq	Direct-quadrature reference frame
Parameters	
R	Resistance filter
L	Inductance filter
C	Capacitance filter

Variables

i_{dq}	Output currents of VSC in the *dq* frame
i_{Ldq}	Load currents in the *dq* frame
e_{dq}	Output voltages of VSC in the *dq* frame
m_{dq}	modulation indexes in the *dq* frame
$\mathbf{x} \in R^n$	State vector
$\tilde{x} \in R^n$	State vector with incremental variables
$\mathbf{u} \in R^m$	Control input vector
$\mathbf{z} \in R^m$	auxiliary variable vector
$\mathbf{R} \in R^{n \times n}$	Inertia matrix
$\mathbf{R} \in R^{n \times n}$	Damping matrix
$\mathbf{J} \in R^{n \times n}$	Interconnection matrix
$\mathbf{g} \in R^{n \times m}$	Input matrix
$H(\mathbf{x})$	Energy storage function
$V(\mathbf{x})$	Candidate Lyapunov function
$K_p \in R^{m \times m}$	Proportional gain matrix
$K_I \in R^{m \times m}$	Integral gain matrix

References

1. Ellabban, O.; Abu-Rub, H.; Blaabjerg, F. Renewable energy resources: Current status, future prospects and their enabling technology. *Renew. Sustain. Energy Rev.* **2014**, *39*, 748–764, doi:10.1016/j.rser.2014.07.113.

2. Bueno-Lopez, M.; Lemos, S.G. Electrification in non-interconnected areas: Towards a new vision of rurality in Colombia. *IEEE Technol. Soc. Mag.* **2017**, *36*, 73–79.

3. Montoya, O.D.; Garcés, A.; Serra, F.M. DERs integration in microgrids using VSCs via proportional feedback linearization control: Supercapacitors and distributed generators. *J. Energy Storage* **2018**, *16*, 250–258, doi:10.1016/j.est.2018.01.014.

4. Zou, P.; Chen, Q.; Xia, Q.; He, G.; Kang, C. Evaluating the Contribution of Energy Storages to Support Large-Scale Renewable Generation in Joint Energy and Ancillary Service Markets. *IEEE Trans. Sustain. Energy* **2016**, *7*, 808–818, doi:10.1109/TSTE.2015.2497283.

5. Justo, J.J.; Mwasilu, F.; Lee, J.; Jung, J.W. AC-microgrids versus DC-microgrids with distributed energy resources: A review. *Renew. Sustain. Energy Rev.* **2013**, *24*, 387–405, doi:10.1016/j.rser.2013.03.067.

6. Kumar, D.; Zare, F.; Ghosh, A. DC Microgrid Technology: System Architectures, AC Grid Interfaces, Grounding Schemes, Power Quality, Communication Networks, Applications, and Standardizations Aspects. *IEEE Access* **2017**, *5*, 12230–12256, doi:10.1109/ACCESS.2017.2705914.

7. Gavriluta, C.; Candela, I.; Citro, C.; Luna, A.; Rodriguez, P. Design considerations for primary control in multi-terminal VSC-HVDC grids. *Electr. Power Syst. Res.* **2015**, *122*, 33–41, doi:10.1016/j.epsr.2014.12.020.

8. Gil-González, W.; Montoya, O.D.; Garces, A. Direct power control for VSC-HVDC systems: An application of the global tracking passivity-based PI approach. *Int. J. Electr. Power Energy Syst.* **2019**, *110*, 588–597, doi:10.1016/j.ijepes.2019.03.042.

9. Ornelas-Tellez, F.; Rico-Melgoza, J.J.; Espinosa-Juarez, E.; Sanchez, E.N. Optimal and Robust Control in DC Microgrids. *IEEE Trans. Smart Grid* **2018**, *9*, 5543–5553, doi:10.1109/TSG.2017.2690566.

10. Roy, T.K.; Mahmud, M.A.; Oo, A.M.T.; Haque, M.E.; Muttaqi, K.M.; Mendis, N. Nonlinear Adaptive Backstepping Controller Design for Islanded DC Microgrids. *IEEE Trans. Ind. Appl.* **2018**, *54*, 2857–2873, doi:10.1109/TIA.2018.2800680.

11. Garces, A. Uniqueness of the power flow solutions in low voltage direct current grids. *Electr. Power Syst. Res.* **2017**, *151*, 149–153, doi:10.1016/j.epsr.2017.05.031.

12. Opiyo, N.N. A comparison of DC- versus AC-based minigrids for cost-effective electrification of rural developing communities. *Energy Rep.* **2019**, *5*, 398–408, doi:10.1016/j.egyr.2019.04.001.

13. Serra, F.M.; Angelo, C.H.D. IDA-PBC controller design for grid connected Front End Converters under non-ideal grid conditions. *Electr. Power Syst. Res.* **2017**, *142*, 12–19, doi:10.1016/j.epsr.2016.08.041.

14. Montoya, O.D.; Gil-González, W.; Serra, F.M. PBC Approach for SMES Devices in Electric Distribution Networks. *IEEE Trans. Circuits Syst. II* **2018**, *65*, 2003–2007, doi:10.1109/TCSII.2018.2805774.

15. Han, J.; Liu, Z.; Liang, N.; Song, Q.; Li, P. An Autonomous Power-Frequency Control Strategy Based on Load Virtual Synchronous Generator. *Processes* **2020**, *8*, 433, doi:10.3390/pr8040433.

16. Serra, F.M.; Angelo, C.H.D.; Forchetti, D.G. IDA-PBC control of a DC–AC converter for sinusoidal three-phase voltage generation. *Int. J. Electron.* **2017**, *104*, 93–110, doi:10.1080/00207217.2016.1191087.

17. Ye, Y.; Zhou, K.; Zhang, B.; Wang, D.; Wang, J. High-Performance Repetitive Control of PWM DC-AC Converters With Real-Time Phase-Lead FIR Filter. *IEEE Trans. Circuits Syst. II* **2006**, *53*, 768–772, doi:10.1109/TCSII.2006.875383.

18. Khefifi, N.; Houari, A.; Machmoum, M.; Ghanes, M.; Ait-Ahmed, M. Control of grid forming inverter based on robust IDA-PBC for power quality enhancement. *Sustain. Energy Grids Netw.* **2019**, *20*, 100276, doi:10.1016/j.segan.2019.100276.

19. Amin, W.T.; Montoya, O.D.; Garrido, V.M.; Gil-González, W.; Garces, A. Voltage and Frequency Regulation on Isolated AC Three-phase Microgrids via s-DERs. In Proceedings of the 2019 IEEE Green Technologies Conference (GreenTech), Lafayette, LA, USA, 3–6 April 2019; pp. 1–6.

20. Huang, X.; Wang, K.; Li, G.; Zhang, H. Virtual Inertia-Based Control Strategy of Two-Stage Photovoltaic Inverters for Frequency Support in Islanded Micro-Grid. *Electronics* **2018**, *7*, 340, doi:10.3390/electronics7110340.

21. Fang, J.; Lin, P.; Li, H.; Yang, Y.; Tang, Y. An Improved Virtual Inertia Control for Three-Phase Voltage Source Converters Connected to a Weak Grid. *IEEE Trans. Power Electron.* **2019**, *34*, 8660–8670.

22. Haque, M.E.; Negnevitsky, M.; Muttaqi, K.M. A Novel Control Strategy for a Variable-Speed Wind Turbine With a Permanent-Magnet Synchronous Generator. *IEEE Trans. Ind. Appl.* **2010**, *46*, 331–339, doi:10.1109/TIA.2009.2036550.

23. Kim, D.; Lee, D. Feedback Linearization Control of Three-Phase UPS Inverter Systems. *IEEE Trans. Ind. Electron.* **2010**, *57*, 963–968, doi:10.1109/TIE.2009.2038404.

24. Loh, P.C.; Newman, M.J.; Zmood, D.N.; Holmes, D.G. A comparative analysis of multiloop voltage regulation strategies for single and three-phase UPS systems. *IEEE Trans. Power Electron.* **2003**, *18*, 1176–1185, doi:10.1109/TPEL.2003.816199.

25. Mattavelli, P. Synchronous-frame harmonic control for high-performance AC power supplies. *IEEE Trans. Ind. Appl.* **2001**, *37*, 864–872, doi:10.1109/28.924769.

26. Lidozzi, A.; Calzo, G.L.; Solero, L.; Crescimbini, F. Integral-resonant control for stand-alone voltage source inverters. *IET Power Electron.* **2013**, *7*, 271–278.

27. Mohamed, I.S.; Zaid, S.A.; Elsayed, H.M.; Abu-Elyazeed, M. Three-phase inverter with output LC filter using predictive control for UPS applications. In Proceedings of the 2013 International Conference on Control, Decision and Information Technologies (CoDIT), Hammamet, Tunisia, 6–8 May 2013; IEEE: Piscataway, NJ, USA, 2013, pp. 489–494.

28. Talbi, B.; Krim, F.; Laib, A.; Sahli, A. Model predictive voltage control of a single-phase inverter with output LC filter for stand-alone renewable energy systems. *Electr. Eng.* **2020**, doi:10.1007/s00202-020-00936-5.

29. Valderrama, G.E.; Stankovic, A.M.; Mattavelli, P. Dissipativity-based adaptive and robust control of UPS in unbalanced operation. *IEEE Trans. Power Electron.* **2003**, *18*, 1056–1062, doi:10.1109/TPEL.2003.813768.

30. Ortega, R.; van der Schaft, A.; Maschke, B.; Escobar, G. Interconnection and damping assignment passivity-based control of port-controlled Hamiltonian systems. *Automatica* **2002**, *38*, 585–596, doi:10.1016/S0005-1098(01)00278-3.

31. Perez, M.; Ortega, R.; Espinoza, J.R. Passivity-based PI control of switched power converters. *IEEE Trans. Control Syst. Technol.* **2004**, *12*, 881–890, doi:10.1109/TCST.2004.833628.

32. Cisneros, R.; Pirro, M.; Bergna, G.; Ortega, R.; Ippoliti, G.; Molinas, M. Global tracking passivity-based PI control of bilinear systems: Application to the interleaved boost and modular multilevel converters. *Control Eng. Pract.* **2015**, *43*, 109–119, doi:10.1016/j.conengprac.2015.07.002.

33. Gil-González, W.; Montoya, O.D.; Garces, A. Control of a SMES for mitigating subsynchronous oscillations in power systems: A PBC-PI approach. *J. Energy Storage* **2018**, *20*, 163–172, doi:10.1016/j.est.2018.09.001.

34. Cisneros, R.; Mancilla-David, F.; Ortega, R. Passivity-Based Control of a Grid-Connected Small-Scale Windmill With Limited Control Authority. *IEEE J. Emerg. Sel. Top. Power Electron.* **2013**, *1*, 247–259, doi:10.1109/JESTPE.2013.2285376.

35. Montoya, O.D.; Gil-González, W.; Garces, A. Distributed energy resources integration in single-phase microgrids: An application of IDA-PBC and PI-PBC approaches. *Int. J. Electr. Power Energy Syst.* **2019**, *112*, 221–231, doi:10.1016/j.ijepes.2019.04.046.

36. Montoya, O.D.; Gil-González, W.; Avila-Becerril, S.; Garces, A.; Espinosa-Pérez, G. Integración de REDs en Redes AC: Una Familia de Controladores Basados en Pasividad. *Revista Iberoamericana De Automática E Informática Industrial* **2019**, *16*, 212, doi:10.4995/riai.2018.10666.

37. Montoya, O.D.; Garces, A.; Avila-Becerril, S.; Espinosa-Pérez, G.; Serra, F.M. Stability Analysis of Single-Phase Low-Voltage AC Microgrids With Constant Power Terminals. *IEEE Trans. Circuits Syst. II Express Briefs* **2019**, *66*, 1212–1216.

38. Luyben, W.L. Tuning Proportional-Integral-Derivative Controllers for Integrator/Deadtime Processes. *Ind. Eng. Chem. Res.* **1996**, *35*, 3480–3483, doi:10.1021/ie9600699.

39. Ruz, M.; Garrido, J.; Vazquez, F.; Morilla, F. Interactive Tuning Tool of Proportional-Integral Controllers for First Order Plus Time Delay Processes. *Symmetry* **2018**, *10*, 569, doi:10.3390/sym10110569.

40. Ahamad, A.; Yadav, C.; Ahuja, S.; Nema, S.; Padhy, P.K. PID tuning procedure based on simplified single parameter optimization. In Proceedings of the 2013 International Conference on Control, Automation, Robotics and Embedded Systems (CARE), Jabalpur, India, 16–18 December 2013; pp. 1–5.

41. Sanchis, R.; Romero, J.A.; Balaguer, P. Tuning of PID controllers based on simplified single parameter optimisation. *Int. J. Control* **2010**, *83*, 1785–1798, doi:10.1080/00207179.2010.495162.

42. Irshad, M.; Ali, A. Optimal tuning rules for PI/PID controllers for inverse response processes. *IFAC-PapersOnLine* **2018**, *51*, 413–418, doi:10.1016/j.ifacol.2018.05.063.

43. Pradhan, R.; Majhi, S.K.; Pradhan, J.K.; Pati, B.B. Antlion optimizer tuned PID controller based on Bode ideal transfer function for automobile cruise control system. *J. Ind. Inf. Integr.* **2018**, *9*, 45–52, doi:10.1016/j.jii.2018.01.002.

44. Meena, D.C.; Devanshu, A. Genetic algorithm tuned PID controller for process control. In Proceedings of the 2017 International Conference on Inventive Systems and Control (ICISC), Coimbatore, India, 19–20 January 2017; pp. 1–6.

45. Barisal, A. Comparative performance analysis of teaching learning based optimization for automatic load frequency control of multi-source power systems. *Int. J. Electr. Power Energy Syst.* **2015**, *66*, 67–77, doi:10.1016/j.ijepes.2014.10.019.

46. Ab. Talib, M.H.; Mat Darns, I.Z. Self-tuning PID controller for active suspension system with hydraulic actuator. In Proceedings of the 2013 IEEE Symposium on Computers Informatics (ISCI), Langkawi, Malaysia, 7–9 April 2013; pp. 86–91.

47. Tejado, I.; Vinagre, B.; Traver, J.; Prieto-Arranz, J.; Nuevo-Gallardo, C. Back to Basics: Meaning of the Parameters of Fractional Order PID Controllers. *Mathematics* **2019**, *7*, 530, doi:10.3390/math7060530.

48. Komurcugil, H. Steady-State Analysis and Passivity-Based Control of Single-Phase PWM Current-Source Inverters. *IEEE Trans. Ind. Electron.* **2010**, *57*, 1026–1030, doi:10.1109/TIE.2009.2025297.

49. He, J.; Li, Y.W. Generalized Closed-Loop Control Schemes with Embedded Virtual Impedances for Voltage Source Converters with LC or LCL Filters. *IEEE Trans. Power Electron.* **2012**, *27*, 1850–1861, doi:10.1109/TPEL.2011.2168427.

50. Peña-Asensio, A.; Arnaltes-Gómez, S.; Rodriguez-Amenedo, J.L.; García-Plaza, M.; Carrasco, J.E.G.; de las Morenas, J.M.A.M. A Voltage and Frequency Control Strategy for Stand-Alone Full Converter Wind Energy Conversion Systems. *Energies* **2018**, *11*, 474, doi:10.3390/en11030474.

51. Sivadas, D.; Vasudevan, K. Stability Analysis of Three-Loop Control for Three-Phase Voltage Source Inverter Interfaced to the Grid Based on State Variable Estimation. *IEEE Trans. Ind. Appl.* **2018**, *54*, 6508–6518, doi:10.1109/TIA.2018.2856846.

52. Gil-González, W.; Serra, F.M.; Montoya, O.D.; Ramírez, C.A.; Orozco-Henao, C. Direct Power Compensation in AC Distribution Networks with SCES Systems via PI-PBC Approach. *Symmetry* **2020**, *12*, 666, doi:10.3390/sym12040666.

53. Zahid, Z.U.; Lai, J.J.; Huang, X.K.; Madiwale, S.; Hou, J. Damping impact on dynamic analysis of LLC resonant converter. In Proceedings of the 2014 IEEE Applied Power Electronics Conference and Exposition—APEC 2014, Fort Worth, TX, USA, 16–20 March 2014; pp. 2834–2841.

54. Serra, F.M.; Angelo, C.H.D.; Forchetti, D.G. Interconnection and damping assignment control of a three-phase front end converter. *Int. J. Electr. Power Energy Syst.* **2014**, *60*, 317–324, doi:10.1016/j.ijepes.2014.03.033.